Journal of Materials Chemistry

Cite this: J. Mater. Chem., 2011, 21, 7802

www.rsc.org/materials

PAPER

Multilayered ordered mesoporous platinum/titania composite films: does the photocatalytic activity benefit from the film thickness?

Adel A. Ismail,*[a] Detlef W. Bahnemann,[b] Jiri Rathousky,[c] Viktor Yarovyi[d] and Michael Wark[de]

Received 24th January 2011, Accepted 21st March 2011
DOI: 10.1039/c1jm10366k

Multilayered films of TiO_2 with ordered cubic mesoporosity were grown *via* layer-by-layer deposition on a conductive FTO (F-doped SnO_2) substrate by dip-coating and subsequent calcination at 400 °C. Since platinum nanoparticles are known to enhance the photocatalytic activity, they were introduced into the TiO_2 mesopores by pulsed electrodeposition. Additionally, sandwich-like layers with up to five alternating TiO_2 and Pt layers were prepared. The photocatalytic gas-phase oxidation of acetaldehyde served as a test reaction to characterize the activity in the gas phase of both pristine TiO_2 as well as Pt/TiO_2 single- and multilayer films. The ordered mesoporous pristine TiO_2 and Pt/TiO_2 nanocomposites exhibited significantly higher photoactivity than commercial Pilkington Activ™ glass and dense TiO_2 films. Moreover for pristine TiO_2 films, those consisting of three layers (about 650 nm in thickness), were shown to be sufficient to achieve a maximum photonic efficiency of $\zeta = 0.45\%$. For the Pt/TiO_2 system, however, a single-layer film with a total thickness of only about 220 nm exhibited an almost identical activity. Moreover, repetitive experiments demonstrated that the newly prepared photocatalyst films did not suffer from a decrease in the photocatalytic activity, evincing their potential for practical applications.

1. Introduction

Mesoporous TiO_2 in the form of thin films or as powders is an interesting material for photocatalytic applications especially due to their very high specific surface area.[1] Furthermore, the crystalline TiO_2 nanoparticles are embedded within a continuous 3D structure, which is beneficial for an easier catalyst recovery. First ordered mesoporous materials for photocatalysis were prepared by doping mesoporous silica with TiO_2.[2] The obtained promising results stimulated efforts for the preparation of pristine TiO_2 with highly ordered mesoporosity and high crystallinity of the walls.[3] The uniform 3D pore system of cubic mesoporous TiO_2 favors the mass-transfer kinetics, which enhances its potential for environmental applications.[4,5] Noble metals such as Pt, Pd, Ag and Au deposited on TiO_2 can act as sinks for photoexcited electrons, hindering the recombination of charge carriers (electrons and holes).[6,7] An ordered mesoporous TiO_2 network with its large external surface area can enhance the photocatalytic activity, *i.e.*, the photonic efficiency, due to several effects: (i) multiple scattering effects, (ii) stabilization of a high dispersion of the noble metal nanocrystals, and (iii) enabling highly efficient electron transport *via* the network of interconnected TiO_2 nanocrystals (antenna effect).[8,9] Additionally, as the gas–solid photocatalytic reactions are surface-based processes,[8] the large surface area provides more adsorption sites for reactant molecules, increasing the efficiency of the majority of photocatalytic processes.

In general, TiO_2 thin films exhibit several unique photocatalytic properties, such as their self-cleaning, antifouling, and anti-bacterial ability. For self-cleaning applications, TiO_2 is deposited on a substrate as a thin film with a few tens of nanometres to a few micrometres in thickness.[10] The pollutants are photocatalytically removed, *e.g.*, by the absorption of sunlight.[11] In addition to the photocatalytic processes, the light-induced hydrophilic properties of the TiO_2 facilitate the removal of dust or inorganic degradation by-products by rainwater. CH_3CHO, being a toxic compound and known to be one of the principal odor-causing gases in indoor air, forms in considerable amounts inside of buildings upon oxidation of organic compounds released by furniture, carpets and cigarette smoke by ozone.[12] The photocatalytic oxidation of CH_3CHO using TiO_2-based catalysts has been proposed to proceed *via* a radical chain reaction mechanism.[13] Investigations employing ^{13}C labelled CH_3CHO revealed that gaseous acetaldehyde is oxidized

[a]*Advanced Materials Department, Central Metallurgical R&D Institute (CMRDI), PO Box 87, Helwan, Cairo, 11421, Egypt. E-mail: aismail@cmrdi.sci.eg; adelali11@yahoo.com*
[b]*Institut für Technische Chemie, Leibniz Universität Hannover, Callinstrasse 3, 30167 Hannover, Germany*
[c]*J. Heyrovsky Institute of Physical Chemistry, v.v.i., Academy of Sciences of the Czech Republic, Dolejskova 3, CZ-18223 Prague 8, Czech Republic*
[d]*Institut für Physikalische Chemie and Elektrochemie, Leibniz Universität Hannover, Callinstrasse 3a, 30167 Hannover, Germany*
[e]*Institut für Technische Chemie, Ruhr-Universität Bochum, Universitätsstrasse 150, 44801 Bochum, Germany*

preferentially into acetic acid, which is immediately oxidized to CO_2, and into HCHO followed by its fast oxidation into CO_2 with HCOOH being the intermediate.[13c,d] The photooxidation of CH_3CHO has been widely investigated on many forms of TiO_2[14] such as powder,[15] thin films,[16] and porous solids.[17] Multilayer coatings of TiO_2 nanoparticles[18] are useful for various applications needing *e.g.*, transparency or easy recovering. However, for practical reasons the number of layers and consequently the number of steps in their fabrication, *e.g.*, by dip-coating, should be kept as small as possible.[19]

The present study is aimed at the enhancement of photocatalytic activity of sol–gel prepared TiO_2 multilayer films with ordered cubic mesoporosity deposited on conductive FTO substrates resulting from the introduction of platinum nanoparticles into the mesopore channels by pulsed electrodeposition. The photocatalytic activity for the oxidation of CH_3CHO in the gas phase was determined for both, pristine TiO_2 and Pt/TiO_2 multilayer films, and compared with that of commercial Pilkington Activ™ glass. To the best of our knowledge, this is the first report on the synthesis of mesoporous TiO_2/Pt composites and on their photonic efficiency.

2. Experimental section

2.1. Materials

Pluronic P123 (a poly(ethylene oxide)–poly(propylene oxide)–poly(ethylene oxide) block copolymer $EO_{20}PO_{70}$-EO_{20}, Aldrich) served as a structure-directing agent. HCl, titanium(IV) tetraethoxide (95%), ethanol and H_2PtCl_6 were purchased from Aldrich and used as received.

2.2. Synthesis of mesoporous multilayer films

Cubic mesoporous titania single-layer films were prepared according to Alberius *et al.*[20] 5 g of Pluronic P123 were added to 60 g of ethanol with stirring for 1 h. Separately, a mixture of 17.6 g titanium ethoxide and 11.25 g of HCl was stirred vigorously for 10 min, resulting in a clear solution. The two mixtures were then combined and stirred for 3 h. Conductive FTO glass slides were coated with the sol prepared at the withdrawal rate of 1 mm s^{-1}. After aging in air for 24 h, the samples were calcined in air at 400 °C for 4 h (heating rate: 1 °C min^{-1}). Multiple-coated films were prepared by repeating the deposition process, being heated at 350 °C for 1 h prior to the subsequent coating step. Finally, the films were calcined at 400 °C for 4 h. For comparison pure non-porous TiO_2 (SG-TiO_2) was prepared by the same sol–gel route but without addition of the structure directing agent Pluronic P123.

2.3. Electrochemical deposition of platinum

The electrochemical experiments were performed using a potentiostat/galvanostat (Autolab 12, Eco Chemie) with GPES software for the collection and analysis of data. A conventional three-electrode cell was used, either mesoporous TiO_2 or dense SG-TiO_2 thin films, a Pt wire and a saturated calomel electrode (SCE) serving as working, counter and reference electrodes, respectively. Platinum was electrochemically deposited from a 10^{-3} M H_2PtCl_6 solution by applying pulses of (*vs.* SCE) 1 s duration interrupted by breaks of 5 s in order to allow diffusion of the Pt^{2+} ions into the pores of the porous films. The total charge amount and deposition current density were 1.2 C cm^{-2} and 5 mA cm^{-2}, respectively. After the electrodeposition, the samples were thoroughly rinsed with deionized water and dried in air.

2.4. Sandwich Pt/TiO_2 multilayer

In multilayer films Pt was electrodeposited by applying 5 pulses of 1 s duration after preparation of each mesoporous TiO_2 layer. The TiO_2 layers were prepared according to the above method and were treated at 350 °C for 1 h prior to the electrodeposition. This procedure was repeated to obtain the required number of TiO_2/Pt double-layers. Finally, the film was treated at 400 °C for 4 h.

2.5. Characterization

Transmission electron microscopy (TEM) was performed at 200 kV with a JEOL JEM-2100F-UHR field-emission instrument equipped with a Gatan GIF 2001 energy filter and a 1K-CCD camera to obtain EEL spectra. Small angle X-ray diffraction (SXRD) patterns were recorded on a Bruker D8 Advance. The film thickness was determined by a Dektak 6 M stylus (Veeco) surface profile measuring system. The texture properties of the films were determined by the analysis of adsorption isotherms of Kr at −196 °C measured with a Micromeritics ASAP 2010 volumetric adsorption unit by the method given in ref. 21. In order to determine texture parameters of thin porous films deposited on supports, whose total surface area is in the range of several tens of square centimetres, the highly sensitive Kr adsorption technique has to be used. To take into account the differing film sizes and thicknesses, all the texture parameters were related to a unit (*i.e.*, 1 cm^3) of the total film volume, which includes both the voids and the pore walls. The specific surface area was determined by the BET method using the molecular cross-sectional area of Kr of 0.21 nm^2. The information on the pore volume was obtained from the limiting adsorption at pressure near to the saturation pressure. The porosity of the films was calculated by dividing the pore volume by the total film volume. As the analysis of adsorption isotherms of Kr at −196 °C is far from being straightforward and a well-established procedure (*e.g.* DFT) has not been implemented yet, a simple method based on comparative plots was used to calculate the mean diameters of the mesopores (D) and the pore size distribution.[21] As a suitable reference material a non-porous anatase (Aldrich) was used, whose surface area was 11.2 m^2 g^{-1}. Comparison plots for each sample were constructed, in which the adsorption on the sample under study was plotted against that on the reference material. The differentiation of obtained plots provided an assessment of the pore size distribution for each film.[21]

The reflectance spectra of the samples in a range of 200–800 nm were recorded with a Varian Cary 100 Scan UV-vis system equipped with a Labsphere integrating sphere diffuse reflectance accessory. The optical band gap energy for each sample was estimated according to the Tauc plot:

$$\alpha = A(h\nu - E_g)^n/h\nu \quad (1)$$

with E_g being the optical band gap, α the absorption coefficient, A a proportional constant, $h\nu$ the energy of a photon, and $n = 2$ used for semiconductors with indirect electronic band transition as TiO_2. Since the absorption coefficient α is proportional to the Kubelka–Munk function $F(R)$, the band gap energy can be obtained from the extrapolation of the linear portion of the plot of $[F(R)h\nu]^{1/2}$ *vs.* $h\nu$ near the onset of absorption edge to the energy axis. As straight lines were obtained in photon energy ranges close to the absorption thresholds, the electronic transition near the band gap was confirmed to be indirect.

2.6. Measurement of the photonic efficiencies in the gas phase

The photocatalytic degradation of CH_3CHO was investigated employing an experimental setup consisting of a gas supply, a photoreactor, and a Syntech Spectras GC 955 gas chromatograph. The illuminated area of each TiO_2-coated sample was 15 cm^2. Each film was pretreated under UV(A) irradiation (2 mW cm^{-2}) for 24 h to clean its surface. The gaseous reaction mixture was prepared by mixing streams of dry air (500 mL min^{-1}), wet air (500 mL min^{-1}, relative humidity of 100%), and 200 ppm CH_3CHO/N_2 (approximately 2.5 mL min^{-1}), to obtain a final CH_3CHO concentration of 450 ppb at a relative humidity of 50% at 297 K. The photoreactor was illuminated with four UV(A) lamps ($\lambda < 380$ nm), the total UV light intensity at 350 nm being 1 mW cm^{-2}. Prior to the photocatalytic tests, the photoreactor was purged with the CH_3CHO/water vapour/air mixture without illumination until a steady CH_3CHO concentration was achieved at the outlet. Afterwards, the sample was irradiated for 120 min. For each measurement the photonic efficiency ζ, which is defined as the ratio of the degradation rate of CH_3CHO and the incident photon flux related to the illuminated area, was calculated according to:

$$\xi = \frac{hcN_A\Delta n}{\phi A\lambda} \quad (2)$$

with h being Planck's constant, c the light velocity, N_A Avogadro's constant, Δn the difference between inlet and outlet flux of CH_3CHO, Φ the light intensity, A the illuminated area, and λ the wavelength of the UV light. Complete degradation of CH_3CHO with an initial concentration of 450 ppb, which corresponds to $\Delta n = 3.03 \times 10^{-10}$ mol s^{-1}, results in a theoretical photonic efficiency ξ_{th} of 0.71%. The efficiency was calculated from steady-state concentrations obtained after 120 min.

3. Results and discussions

3.1. Structural investigations

Since the photocatalytic activity of single-layer mesoporous TiO_2 films is expected to be too low, mesoporous multilayer TiO_2 films have been synthesized and subsequently loaded with Pt nanoparticles. Concerning the electrochemical Pt loading, two different methods were performed, either the loading as a final step on a multilayer film (up to five mesoporous TiO_2 layers) or Pt deposition directly after each dip-coating step (sandwich structures). By the second route, sandwich structures consisting of up to five TiO_2 and five Pt layers on FTO substrate were prepared. During the heat treatment after the dip-coating steps, TiO_2 cross-links and starts to crystallize, and at the same time the surfactant is removed, leaving the mesoporous TiO_2 material.[20] The ordering of the formed mesoporous multilayer Pt/TiO_2 nanocomposites was characterized by the small angle X-ray scattering (Fig. 1A). The as-made sample exhibits an intensive peak, which can be indexed as the (100) Bragg reflection of the *Im*3*m* space group[20] and a weak hump which might indicate the (200) reflection. Calcination at 400 °C leads to a shrinkage of the pores as indicated by a shift of the (100) reflection to higher 2θ angles (diffractogram (a) in Fig. 1B). Such shrinkage is typical for this type of structured mesoporous layers.[20,22] With the deposition of additional layers, the disorder of the structure increases as follows: from the broadening of the reflection ((b) in Fig. 1B) and decrease in its intensity ((c–e) in Fig. 1B). The increasing disorder is due to the repeated calcinations included in the preparation protocol of the multilayer films.

The adsorption isotherms of Kr at 77 K in Fig. 2 show the influence of the deposition of different amounts of Pt on the porosity of one-layer and three-layer films (Fig. 2a and b). Also a sample prepared by layer-by-layer deposition (three layers of each TiO_2 and Pt) is included. All the isotherms are of the IUPAC type IV confirming the mesoporosity of all the samples measured. The texture data are given in Table 1. The comparison of the pristine calcined one-layer film with those loaded with 5 and 30 pulses (Fig. 2a and Table 1) shows that the specific surface area, porosity and very slightly also the pore width decrease with increasing number of pulses, which corresponds to an increasing amount of incorporated platinum. The introduction of Pt particles does not lead to any deterioration of the porosity. Only the pristine and 5 pulses Pt films exhibit a slightly broader pore size distribution, while those of samples containing even larger amounts of Pt exhibit rather narrow pore size distribution, *e.g.* the sample 30 pulses Pt/TiO_2. Concerning the pore size

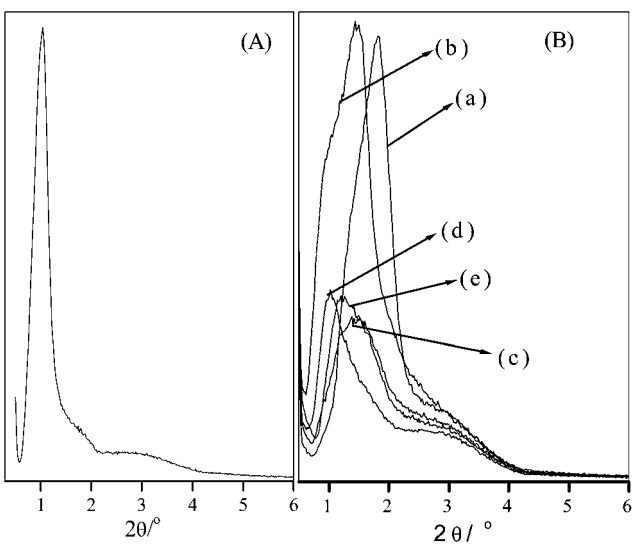

Fig. 1 SAXS pattern of as made cubic mesoporous TiO_2 (A), SAXS patterns of multilayer films of mesoporous TiO_2 calcined at 400 °C (B): one layer TiO_2 (a), two layer TiO_2 (b), three layer TiO_2 (c), four layer TiO_2 (d) and five layer TiO_2 (e).

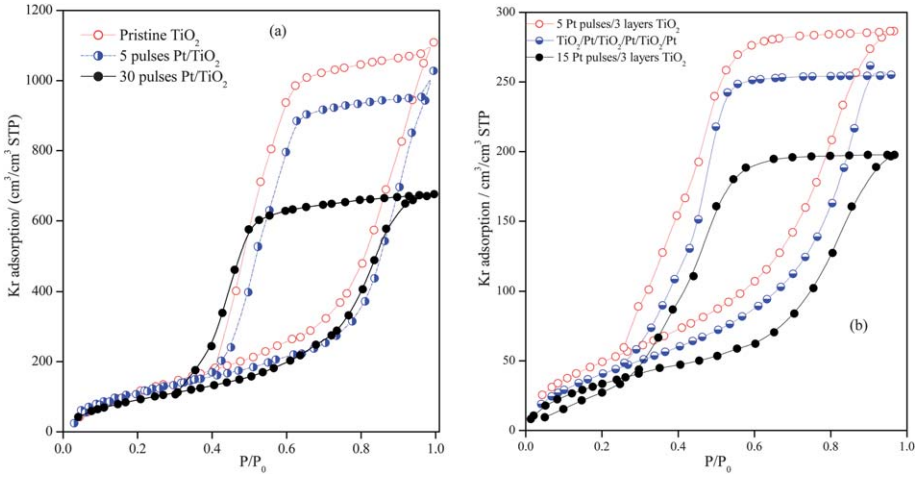

Fig. 2 Kr adsorption isotherms of pristine mesoporous TiO_2 thin films and of 5 and 30 pulses Pt/TiO_2 thin films (a). Kr adsorption isotherms of mesoporous at 5 pulses Pt/3 layer TiO_2 and 3 layer Pt (5 pulses)–3 layer TiO_2 like sandwich unit thin film and 15 pulses Pt/3 layer TiO_2 (b).

corresponding to the maximum of the pore size distribution, there is only a very slight decrease due to the introduction of Pt from about 10 to 9–9.5 nm. In principle the same holds for the three layer films doped with 5 and 15 pulses (Fig. 2b and Table 2) showing that also on a three-layer film the Kr adsorption capacity decreases with the number of pulses applied in the electrochemical deposition of Pt. Again, the more Pt is deposited the more pore volume decreases. This demonstrates that Pt is really deposited within the pores, because in case of a pore blocking by a continuous layer of Pt on the external surface a more drastic decrease in the Kr adsorption must be expected. However, the comparison of the single-layer film doped with 5 pulses (Fig. 2a) with a three-layer film one time doped with 5 pulses (Fig. 2b) shows that both the specific surface area and porosity drastically decrease with the number of TiO_2 layers present. The reason is the repeated calcination included for the preparation of the multilayer films. If the deposition of Pt by applying 15 pulses in either one step on a three-layer TiO_2 film or in three steps of 5 pulses after formation of each of the three TiO_2 layers (sandwich configuration) is compared by Kr adsorption (Fig. 2b) it is clearly visible that with the repeated deposition more pore volume remains accessible.

In the case of single-layer TiO_2 films calcined at 400 °C TEM cross-section images confirm the preservation of the worm-like mesoporous structure even after deposition of Pt by applying 5 pulses (Fig. 3b). In a sample on which 5 pulses are applied Pt nanoparticles are hardly visible, indicating that their diameter must be below approximately 5 nm. Due to the high conductivity of the TiO_2 framework[23] the Pt particles are well distributed over the whole film. After applying 30 pulses, however, agglomerates of Pt within the TiO_2 layer become clearly visible (Fig. 3d). Close to the Pt nucleation centres formed in the first few pulses more and more Pt is deposited leading to the large aggregates. The generation of the Pt aggregates after application of 15 or 30 pulses is also indicated by a change in the colour of the films, appearing more and more grey. With progressive electrochemical deposition as a result of combined nucleation and growth, finally the Pt nanostructures might fill the pores and thus form a replica of the pore system. This has already been observed for the deposition of Au nanostructures.[23] On high-resolution TEM (HR-TEM) images the different Pt and TiO_2 particles are visible already after electrodeposition of 5 pulses (Fig. 3a). The atomic planes of the Pt particles are separated by 2.2 Å, which agrees with the (111) lattice spacing (2.2 Å) of face-centered cubic Pt; crystalline TiO_2 anatase particles are indicated by the typical (101, 3.5 Å) and (103, 2.4 Å) lattice fringes. The appearance of the (111) planes of the Pt particles within the mesostructured TiO_2 gives direct evidence that the nanoparticles are effectively

Table 1 Texture and photocatalytic properties of pristine TiO_2 and Pt/TiO_2 mesoporous films[a]

Pt pulses	Thickness/nm	S_{spec}/m^2 cm^{-3}	V_{spec}/cm^3 cm^{-3}	Porosity (%)	D_{max}/nm	Θ/°	Rate/$\times 10^{11}$ mol s^{-1}	ξ (%)
0	179 ± 18	352	0.53	53	10	13.6 ± 2	4.9	0.15
1	188 ± 16	—	—	—	—	10 ± 0.5	5.6	0.23
2	199 ± 20	—	—	—	—	10 ± 0.5	16.4	0.38
5	224 ± 19	302	0.44	44	10	8.7 ± 0.5	18.5	0.44
15	248 ± 18	—	—	—	—	<5	9.71	0.24
30	267 ± 20	247	0.42	42	9	<5	9.04	0.01
SG-TiO_2	200 ± 15					11.6 ± 3	3.03	0.07
Pt/SG-TiO_2	220 ± 18					9.3 ± 1	10.79	0.24

[a] S_{spec}, the specific surface area of the film. D_{max}, the pore width corresponds to the maximum of pore size distribution, practically the same as the mean pore size. R, the initial photocatalytic degradation rate. Θ: Water contact angle, ξ_{rel}, the photonic efficiency.

Table 2 Textural properties of multilayer films of pristine TiO_2 and Pt/TiO_2 nanocomposites at different Pt loadings and their photocatalytic properties (initial rate and photonic efficiency of photocatalytic CH_3CHO degradation)[a]

	Pristine TiO_2				5 Pulses Pt			
TiO_2 layers	Thickness/nm	Rate/$\times 10^{10}$ mol s^{-1}	Θ/°	ξ (%)	Thickness/ nm	Rate/$\times 10^{10}$ mol s^{-1}	Θ/°	ξ (%)
1	179 ± 20	1.15	13.6 ± 2	0.15	224 ± 20	1.73	8.3 ± 0.5	0.44
2	447 ± 20	1.39	10.6 ± 2	0.30	521 ± 25	1.78	7.2 ± 0.5	0.43
3	654 ± 25	1.95	13 ± 2	0.43	677 ± 40	1.95	4.3 ± 0.5	0.46
4	848 ± 50	1.92	12.4 ± 2	0.44	888 ± 60	1.69	6.2 ± 1	0.45
5	1121 ± 75	2.0	14.9 ± 2	0.45	1135 ± 60	1.92	7.4 ± 2	0.46

[a] Θ, Water contact angle, ξ_{rel}, the relative photonic efficiency.

Table 3 Textural properties of TiO_2-layer-by-Pt-layer sandwich structures and their photocatalytic properties (initial rate and photonic efficiency of photocatalytic CH_3CHO degradation)[a]

No. of layers	Thickness/nm	S_{spec}/m^2 cm^{-3}	V_{spec}/cm^3 cm^{-3}	Porosity (%)	D_{max}/nm	Θ/°	Rate/$\times 10^{10}$ mol s^{-1}	ξ (%)
1	214 ± 10	302	0.44	44	10	8.6 ± 0.5	1.53	0.43
2	502 ± 15	—	—	—	—	7.6 ± 1	1.46	0.44
3	724 ± 25	224	0.35	35	9.3	4.6 ± 0.5	1.68	0.45
4	989 ± 50	—	—	—	—	5.4 ± 1	1.75	0.43
5	1342 ± 80	—	—	—	—	4.7 ± 0.4	1.51	0.44

[a] S_{BET}, the BET surface area of the whole film, V_{spec}, the specific volume of pores, the porosity equal to 100 times the specific volume of pores, D_{max}, the pore width corresponds to the maximum of pore size distribution. Due to the symmetry of the PSD D_{max} is practically the same as the mean pore size. Θ: Water contact angle, ξ_{rel}, the photonic efficiency.

encapsulated in the pores instead of being deposited on the surface of the film. Analysis by EDX measurements revealed Pt : Ti ratios of 0.008, 0.025, and 0.047 after 5, 15 and 30 pulses, respectively.

Multilayer films of Pt/TiO_2 nanocomposites exhibit absorption of ultraviolet (UV) light, which is slightly blue shifted compared to that of bulk TiO_2 with a band gap of about 3.2 eV (Fig. 4). The band gap energy for the mesoporous TiO_2 thin films is about 3.4 eV, which might be a result of the porosity of the mesoporous TiO_2 film.[24] It has been reported that anatase crystallites exhibit bulk physical properties if particle diameters are larger than 5 nm;[25] in the pore walls of the mesoporous films

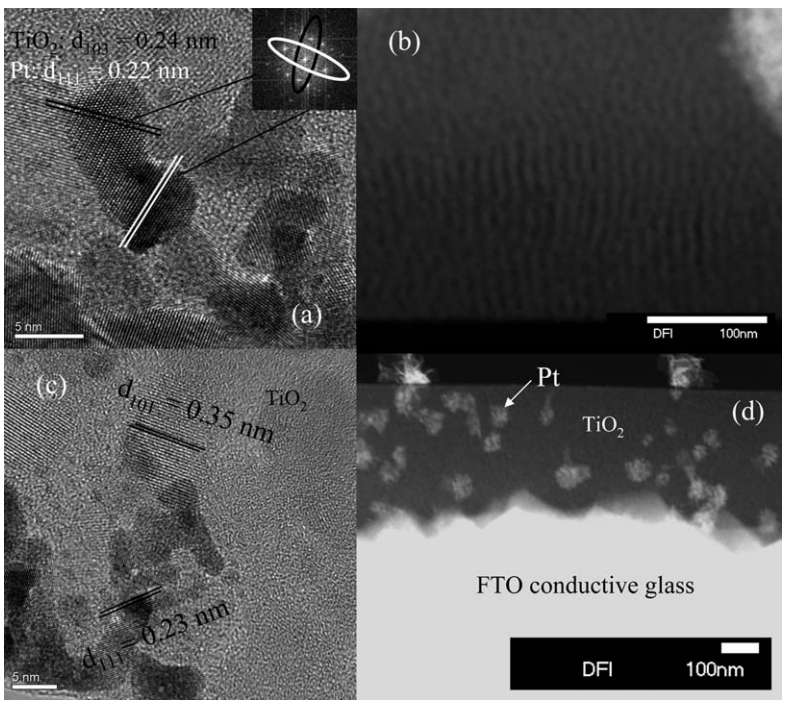

Fig. 3 A representative HR-TEM image of the Pt and TiO_2 nanoparticles in the 15 pulses Pt/TiO_2 thin film (a), TEM images of mesoporous at 30 pulses Pt/TiO_2 thin film (c), the insets show the SAED patterns for the nanocrystalline anatase phase at 400 °C. TEM micrographs of the cross-section of ordered mesoporous TiO_2 films on FTO-coated glass after pulsed electrodeposition of Pt by application of (b) five and (d) 30 pulses.

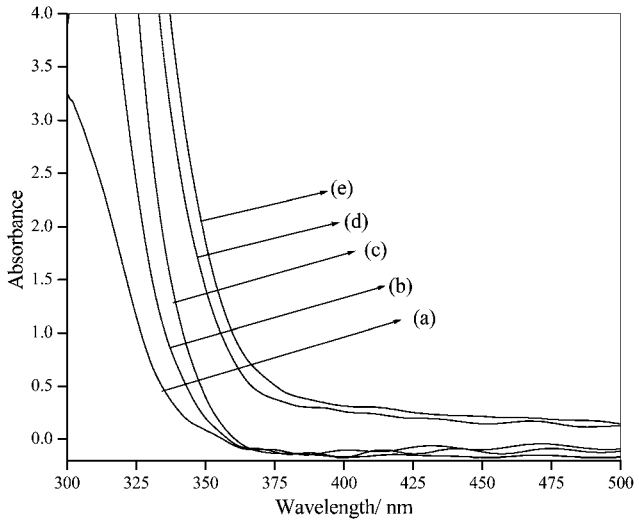

Fig. 4 Absorbance of *n* layer of TiO_2—*n* layer of Pt (*n* = 1–5 times) sandwich units. One layer (a), two layers (b), three layers (c), four layers (d) and five layers (e).

most of the anatase crystallites appear to be smaller. With increased film thickness the absorption edge of the pristine TiO_2 thin films apparently shifts from around 340 nm to around 360 nm for a 5-layer film. A nearly linear absorption edge shift provides convincing evidence for the regular growth of either pristine TiO_2 or Pt/TiO_2 multilayer films.

The wettability of surfaces was characterised by measuring the contact angles of the films and water droplets after exposure to UV light (Tables 1–3). In the dark, the contact angles were determined to be 20–35°. UV-light exposure caused the water-contact angle of the Pt/TiO_2 multilayer films to decrease to <10° within a few hours, thus evincing that the film surface became superhydrophilic.

3.2. Photocatalytic oxidation of acetaldehyde in gas phase

The activity of the multilayer Pt/TiO_2 films was investigated for the photocatalytic oxidation of CH_3CHO in gas phase. CH_3CHO was used as a model for a harmful organic gas. This reaction is photocatalytic on the basis of the fact that both illumination and TiO_2 are needed for the decomposition.[26] The overall process of the photocatalytic CH_3CHO decomposition can be described by the following equation:[27]

$$2CH_3CHO + 5O_2 \xrightarrow[\text{UV light}]{\text{Pt/Tio}_2\text{ film}} 4CO_2 + 4H_2O \qquad (3)$$

It has been shown previously that the photocatalytic oxidation of CH_3CHO occurs on the surface and in the pores of TiO_2 and that molecular O_2 and H_2O are necessary for this purpose. Molecular oxygen adsorbed on the TiO_2 surface prevents the recombination of electron–hole pairs by trapping electrons; superoxide ions are thus formed. ·OH radicals are formed from holes reacting with either H_2O or OH^- adsorbed on the TiO_2 surface. The radicals ·OH and $O_2^{\cdot-}$ are widely accepted as primary oxidants in heterogeneous photocatalysis. These oxidative species can easily oxidize CH_3CHO. The oxidizing power of the ·OH radicals is strong enough to break C–C bonds and C–H bonds of CH_3CHO adsorbed on the surface of TiO_2 leading to the formation of CO_2 and H_2O.[28] As shown in Fig. 5 a direct correlation between the photonic efficiencies and the Pt concentrations is clearly observed. Both, pristine TiO_2 and Pt/TiO_2 prepared with different amounts of pulses already show a considerably higher ability to convert CH_3CHO than Pilkington Active™ glass or dense TiO_2 and Pt/TiO_2 films, respectively, probably due to the much larger surface area of the mesoporous films and its highly crystalline anatase content. The results evince that the photonic efficiency increases with increasing the number of Pt pulses from 1 to 5 with the maximum photonic efficiency being 0.44%. Subsequently, the photonic efficiency gradually decreases with an increasing number of Pt pulses reaching a value of 0.2% for the sample prepared employing 30 Pt pulses.

It has been shown that platinum particles on semiconductor materials readily accept and store electrons, leading to a shift in the Fermi level to a more negative potential.[29] In the present work, 3-D cubic Pt/TiO_2 nanocomposites at 5 Pt pulses showed 3 times higher activity for the photooxidation of CH_3CHO than pristine TiO_2 (Fig. 5 and Table 1). Pt nanoparticles electrodeposited in the pore system of the mesoporous TiO_2 film provide a more efficient charge separation of the electron–hole pairs and an increase in their lifetime. The Fermi level of Pt (E_F = 0.7 V *vs.* NHE)[30] is more positive than the conduction band of energy of TiO_2 (E_{CB} = −0.66 V *vs.* NHE).[31] Hence, the storage of multiple electrons during the charge equilibration with the semiconductor can produce a significant shift in the Fermi level, thus driving the overall Fermi level to more negative potentials. Thereby, it retards efficiently the recombination of the electron–hole pairs formed upon UV(A) light absorption.[31,32] Under these conditions, the Fermi level of the composite shifts closer to the conduction band of the semiconductor. Assuming a Schottky contact between the mesoporous TiO_2 network and the noble metal particle, the Pt particles then serve as active sites for the reduction of molecular oxygen, thus transferring the trapped

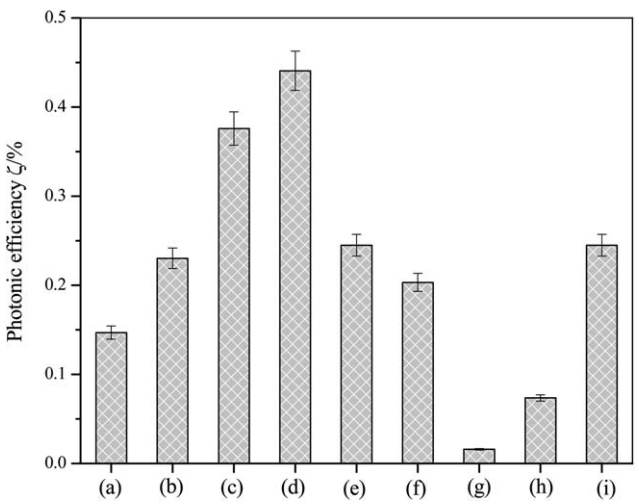

Fig. 5 Dependence of photonic efficiency of mesoporous pristine TiO_2 (a) and Pt/TiO_2 nanocomposite films with Pt loaded by pulsed electrodeposition of 1 pulse (b), 2 pulses (c), 5 pulses (d), 15 pulses (e), 30 pulses (f), commercial Pilkington Activ™ glass photocatalyst (g), SG-TiO_2 (h) and 5 pulses/SG-TiO_2 (i).

photogenerated electrons to adsorbed molecular oxygen producing $O_2^{\cdot-}$ radicals whereas the holes simultaneously accumulate at the metal–oxide interface.[6,33] With the interface being maximal at low platinum loading and high dispersion, too large platinum particles (produced with more than 5 pulses Pt) could also act as recombination centers and become detrimental for photocatalysis by hindering or even avoiding the active photogenerated charge carrier transfer to the reactant species at the surface.[34] Under the experimental conditions employed here 5 pulses Pt is considered to be the optimum and was hence used in the following.

The relationship between the number of layers and the photonic efficiency of pristine TiO_2 and mesoporous Pt/TiO_2 was investigated (Fig. 6 and Table 2). The mesoporous Pt/TiO_2 layer film thickness is approximately 224–1135 nm depending on the number of layers. Our results show that the film thickness increases almost linearly with an increase in the number of dip coatings, which is in agreement with a former report.[35] Fig. 6 shows that for mesoporous pristine TiO_2 the photocatalytic activity increases from ~0.15 to 0.43% with increasing film thickness, reaching a plateau for films with a thickness of around 654 ± 25 nm, *i.e.*, for three-layer films. This observation can be explained by the fact that an increase in the film thickness can lead to an attenuation of the light penetration resulting in decreased photodecomposition rates of CH_3CHO.[36] At large film thickness (four and five layers), a further increase in thickness does not lead to any photoactivity improvement. The photonic efficiency is limited by the diffusion rate of the CH_3CHO gas to the photocatalytically active surface, as a result of the difference in the size and number of pores and thickness of films. For Pt/single-layer TiO_2 the photonic efficiency for the photocatalytic oxidation of CH_3CHO in the gas phase was improved by a factor of 3 as compared to pristine TiO_2 (Fig. 6 and Table 2). With increasing number of TiO_2 layers, we observed that deposition of Pt slightly increased the photonic efficiencies. This is explained by the large-surface of mesoporous Pt/single-layer TiO_2 films (302 m^2 cm^{-3}) being especially effective as the

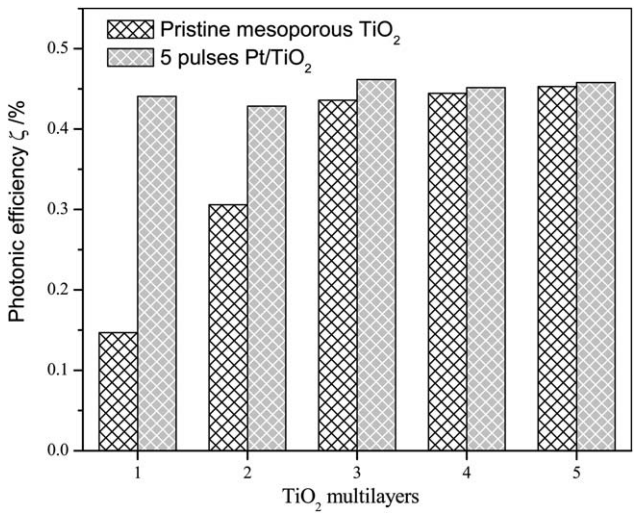

Fig. 6 Comparison of photocatalytic activities of multilayer films of pristine TiO_2 and Pt/TiO_2 nanocomposites for degradation of CH_3CHO in gas phase.

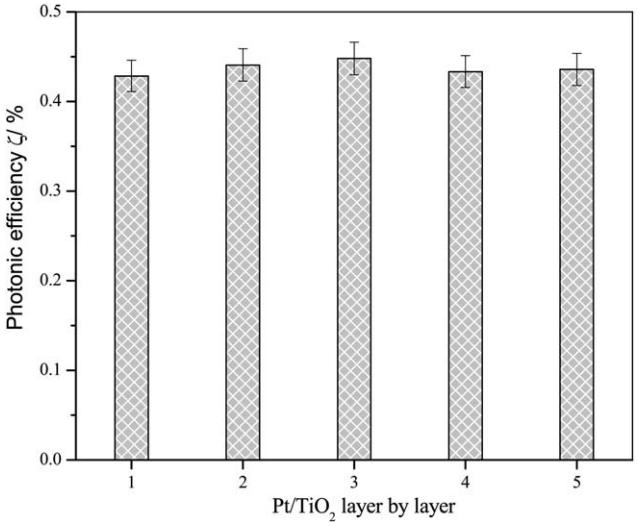

Fig. 7 Influence of TiO_2 layer-by-Pt layer nanocomposites like sandwich unit on photocatalytic degradation of CH_3CHO in the gas phase.

photocatalytic oxidation of CH_3CHO in the gas phase requires the adsorption of the reactants prior to the reaction on the surface. The amount of adsorbed substances is increased in Pt/single-layer TiO_2 due to the large surface area, which enhances the photocatalytic process. In contrast, Pt/three-layer TiO_2 has a surface area and a pore diameter 265 m^2 cm^{-3} and 8.6 nm, respectively. In general, as the film thickness increases, the diffusion time required to reach complete penetration increases. These factors are responsible for the observation that a saturation loading is reached beyond which no further increase in conversion is observed.[36]

The TiO_2-layer-by-Pt-layer sandwich structures have also been investigated concerning their efficiency for the photocatalytic oxidation of CH_3CHO in the gas phase (Fig. 7 and Table 3). The results indicate that there are no significant changes in terms of the photonic efficiency. Actually, these results were unexpected as the increase in the number of TiO_2 and Pt layers should lead to a linear increase in the anatase content. Single-layer Pt/TiO_2 films are, however, already sufficient to obtain maximum photonic efficiency. This may be attributed to the fact that the Pt particle size will continue to grow as a result of the repeated calcinations thus leading to a decrease in the surface area. Thus, the homogeneous distribution of the anatase particles at Pt/single-layer TiO_2 is playing an important role for a good accessibility of molecules from the gas phase. The 3-D mesoporous TiO_2 network acts as an antenna system transferring the initially generated electrons from the location of light absorption to a suitable interface with the noble metal catalyst and subsequently to the location of the Pt nanoparticle where the actual electron transfer reaction will take place. Thus, its acceleration through the electron transfer catalysis induced by the Pt deposits will result in the observed increase in photonic efficiency.[6]

To explore the advantage of 3D mesoporous Pt/TiO_2 nanocomposites and their applicability, reuse cycles of newly prepared photocatalysts were examined for the photooxidation of CH_3CHO (Fig. 8A). Based on the above results, it can be concluded that the 5 pulses Pt/TiO_2 nanocomposites exhibited the highest activity. The recycling tests demonstrated that this

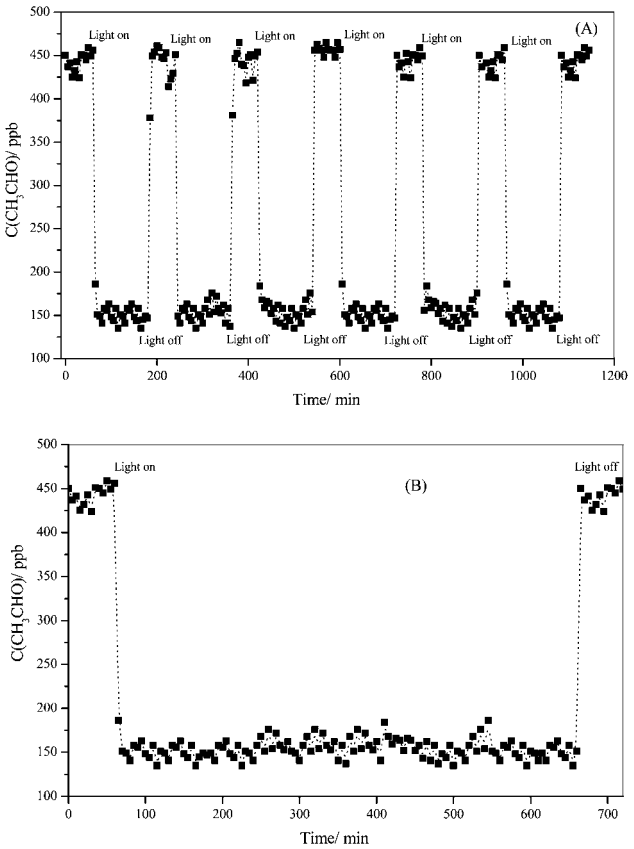

Fig. 8 Recycling test of 5 pulses Pt/one layer TiO_2 calcined at 400 °C repetitively for 5 times (a). Continuous photocatalytic degradation of CH_3CHO in the gas phase for 10 h using 5 pulses Pt/one layer TiO_2 film calcined at 400 °C (b).

photocatalyst was quite stable during that gas–solid heterogeneous photocatalysis since no significant decrease in activity was observed even after being used repetitively for 5 times, showing a good potential for practical applications. In general, the cubic mesoporous Pt/TiO_2 nanocomposites are stable and can be recycled without loss of their photochemical activity. Also, we have continuously carried out the experiments for 10 h (Fig. 8B). The results indicated that the Pt/TiO_2 is photoactive and stable. This clearly demonstrates the added advantages of mesostructural ordering on the photocatalytic properties of TiO_2, which can be attributed to the large accessible surface areas presented in the ordered sample.

4. Conclusions

Highly crystalline, mesoporous pristine TiO_2 and Pt/TiO_2 multilayer films have been synthesized. The results indicated that the deposition of TiO_2 layer-by-layer did not change the mesoporous structure significantly. The photocatalytic removal rate of acetaldehyde showed that meso-ordered pristine TiO_2 is photocatalytically more active than Pilkington Activ™ glass. Also, three-layer mesoporous pristine TiO_2 films exhibit greatly enhanced performance for the photocatalytic oxidation of CH_3CHO that at 654 ± 25 nm thickness was sufficient to achieve a maximum photonic efficiency of 0.45%. Moreover, the deposited Pt particles have been demonstrated to serve as trapping centers for electrons generated in light-activated TiO_2. The improved efficiency and potentially low-cost synthesis suggest that this material might be practically useful as a photocatalyst. The 3-D cubic mesoporous TiO_2 is stable and can be recycled without loss of its photochemical activity.

References

1 (*a*) S. S. Soni, M. J. Henderson, J.-F. Bardeau and A. Gibaud, *Adv. Mater.*, 2008, **20**, 1493–1498; (*b*) E. Allain, S. Besson, C. Durand, M. Moreau, T. Gacoin and J.-P. Boilot, *Adv. Funct. Mater.*, 2007, **17**, 549–554; (*c*) J. Tang, Y. Wu, E. W. McFarland and G. D. Stucky, *Chem. Commun.*, 2004, 1670–1671.

2 (*a*) W. Dong, Y. Sun, C. W. Lee, W. Hua, X. Lu, Y. Shi, S. Zhang, J. Chen and D. Zhao, *J. Am. Chem. Soc.*, 2007, **129**, 13894–13904; (*b*) Z. Wang, F. Zhang, Y. Xue, B. Cui and J. N. Guan, *Chem. Mater.*, 2007, **19**, 3286–3293; (*c*) Y. Li and S.-J. Kim, *J. Phys. Chem. B*, 2005, **109**, 12309–12315; (*d*) Y. Xuzhuang, D. Yang, Z. Huaiyong, L. Jiangwen, W. N. Martins, R. Frost, L. Daniel and S. Yuenian, *J. Phys. Chem. C*, 2009, **113**, 8243–8248.

3 (*a*) E. Martínez-Ferrero, Y. Sakatani, C. Boissière, D. Grosso, A. Fuertes, J. Fraxedas and C. Sanchez, *Adv. Funct. Mater.*, 2007, **17**, 3348–3354; (*b*) A. A. Belhekar, S. V. Awate and R. Anand, *Catal. Commun.*, 2002, **3**, 453; (*c*) S. Zheng, L. Gao, Q. Zhang and J. Guo, *J. Mater. Chem.*, 2000, **10**, 723.

4 (*a*) S. Rodrigues, K. T. Ranjit, S. Uma, I. N. Martyanov and K. J. Klabunde, *Adv. Mater.*, 2005, **17**, 2467; (*b*) J. C. Yu, X. C. Wang and X. Z. Fu, *Chem. Mater.*, 2004, **16**, 1523.

5 (*a*) J. C. Yu, J. Yu and J. Zhao, *Appl. Catal., B*, 2002, **36**, 31; (*b*) M. M. Yusuf, H. Imai and H. Hiraschima, *J. Sol-Gel Sci. Technol.*, 2001, **25**, 65; (*c*) Q. Dai, L. Y. Shi, Y. G. Luo, J. L. Blin, D. J. Li, C. W. Yuan and B. L. Su, *J. Photochem. Photobiol., A*, 2002, **148**, 295; (*d*) E. Stathatos, T. Petrova and P. Lianos, *Langmuir*, 2001, **17**, 5025.

6 (*a*) A. A. Ismail, D. Bahnemann, I. Bannat and M. Wark, *J. Phys. Chem. C*, 2009, **113**, 7429–7435; (*b*) A. A. Ismail, D. Bahnemann, L. Robben, V. Yarvori and M. Wark, *Chem. Mater.*, 2010, **22**, 108–116.

7 (*a*) M. Andersson, H. Birkedal, N. R. Franklin, T. Ostomel, S. Boettcher, A. C. Palmqvist and G. D. Stucky, *Chem. Mater.*, 2005, **17**, 1409–1415; (*b*) X. Wang, J. C. Yu, H. Y. Yip, L. Wu, P. K. Wong and S. Y. Lai, *Chem.–Eur. J.*, 2005, **11**, 2997–3004.

8 M. R. Hoffmann, S. T. Martin, W. Y. Choi and D. W. Bahnemann, *Chem. Rev.*, 1995, **95**, 69.

9 (*a*) A. Hagfeldt and M. Grätzel, *Acc. Chem. Res.*, 2000, **33**, 269; (*b*) Q. H. Yang, M. P. Kapoor and S. Inagaki, *J. Am. Chem. Soc.*, 2002, **124**, 9694.

10 A. Mills, G. Hill, S. Bhopal, I. P. Parkin and S. A. O'Neill, *J. Photochem. Photobiol., A*, 2003, **160**, 185.

11 Y. Paz, Z. Luo, L. Rabenberg and A. Heller, *J. Mater. Res.*, 1995, **10**, 2842.

12 (*a*) R. Reiss, P. B. Ryan, S. J. Tibettes and P. Koutrakis, *J. Air Waste Manage. Assoc.*, 1995, **45**, 811; (*b*) G. Leonardos, D. Kendall and N. Barnard, *J. Air Pollut. Control Assoc.*, 1969, **19**, 91; (*c*) H. Wakeham, *The Chemistry of Tobacco Smoke*, ed. I. Schmeltz, Plenum Press, New York, 1972, vol. 1.

13 (*a*) Y. Zhao, X. T. Zhang, J. Zhai, L. Jiang, Z. Y. Liu, S. Nishimoto, T. Murakami, A. Fujishima and D. B. Zhu, *Microporous Mesoporous Mater.*, 2008, **116**, 710; (*b*) Y. Ohko, D. A. Tryk, K. Hashimoto and A. Fujishima, *J. Phys. Chem. B*, 1998, **102**, 2699; (*c*) D. S. Muggli, J. T. McCue and J. L. Falconer, *J. Catal.*, 1998, **173**, 470; (*d*) X. X. Fan, X. Y. Chen, S. P. Zhu, Z. S. Li, T. Yu, J. H. Ye and Z. G. Zou, *J. Mol. Catal. A: Chem.*, 2008, **284**, 155.

14 (*a*) P. V. Kamat, *J. Phys. Chem. C*, 2007, **111**, 2834; (*b*) X. X. Yang, C. D. Cao, K. Hohn, L. Erickson, R. Maghirang, D. Hamal and K. Klabunde, *J. Catal.*, 2007, **252**, 296; (*c*) H. Kim and W. Choi, *Appl. Catal., B*, 2007, **69**, 127; (*d*) T. Ohno, N. Murakami, T. Tsubota and H. Nishimura, *Appl. Catal., A*, 2008, **349**, 70.

15 (*a*) D. S. Muggli, J. T. McCue and J. T. Falconer, *J. Catal.*, 1998, **173**, 470; (*b*) C. A. Jenkins and D. M. Murphy, *J. Phys. Chem. B*, 1999, **103**, 1019; (*c*) J.-G. Li, C. Tang, D. Li, H. Haneda and T. Ishigaki, *J. Am. Ceram. Soc.*, 2004, **87**, 1358.

16 (*a*) Y. Ohko, D. A. Tryk, K. Hashimoto and A. Fujishima, *J. Phys. Chem. B*, 1998, **102**, 2699; (*b*) M. C. Blount, D. H. Kim and J. L. Falconer, *Environ. Sci. Technol.*, 2001, **35**, 2988; (*c*) T. Kawahara, Y. Konishi, H. Tada, N. Tohge, J. Nishii and S. Ito, *Angew. Chem., Int. Ed.*, 2002, **41**, 2811.

17 (*a*) X. Ye, D. Chen, J. Gossage and K. Li, *J. Photochem. Photobiol., A*, 2006, **183**, 35; (*b*) A. Yamamoto and H. Iami, *J. Catal.*, 2004, **226**, 462.

18 (*a*) A. Nakajima, K. Hashimoto, T. Watanabe, K. Takai, G. Yamauchi and A. Fujishima, *Langmuir*, 2000, **16**, 7044–7047; (*b*) M. Machida, K. Norimoto, T. Watanabe, K. Hashimoto and A. Fujishima, *J. Mater. Sci.*, 1999, **34**, 2569–2574; (*c*) D. Lee, D. Omolade, R. E. Cohen and M. F. Rubner, *Chem. Mater.*, 2007, **19**, 1427–1433.

19 M. Zukalova, A. Zukal, L. Kavan, M. K. Nazeeruddin, P. Liska and M. Grätzel, *Nano Lett.*, 2005, **5**, 1789.

20 P. C. Alberius, K. L. Frindell, R. C. Hayward, E. J. Kramer, G. D. Stucky and B. F. Chmelka, *Chem. Mater.*, 2002, **14**, 3284–3294.

21 (*a*) J. Rathouský, V. Kalousek, V. Yarovyi, M. Wark and J. Jirkovský, *J. Photochem. Photobiol., A*, 2010, **216**, 126; (*b*) J. Rathouský, V. Kalousek, M. Kolář, J. Jirkovský and P. Barták, *Catal. Today*, 2011, **161**, 202.

22 (*a*) E. L. Crepaldi, G. J. d. A. Soler-Illia, D. Grosso, F. Cagnol, F. Ribot and C. Sanchez, *J. Am. Chem. Soc.*, 2003, **125**, 9770; (*b*) D. Grosso, G. J. d. A. Solar-Illia, E. L. Crepaldi, F. Cagnol, C. Sinturel, A. Bourgeois, A. Brunet-Bruneau, H. Amenitsch, P. A. Albouy and C. Sanchez, *Chem. Mater.*, 2003, **15**, 4562.

23 I. Bannat, K. Wessels, T. Oekermann, J. Rathousky, D. Bahnemann and M. Wark, *Chem. Mater.*, 2009, **21**, 1645.

24 Y. Fu, Z. Jin, W. Xue and Z. Ge, *J. Am. Ceram. Soc.*, 2008, **91**, 2676.

25 (*a*) C. Kormann, D. Bahnemann and M. R. Hoffmann, *J. Phys. Chem.*, 1988, **92**, 5196–5201; (*b*) S. Monticone, R. Tufeu, A. V. Kanaev, E. Scolan and C. Sanchez, *Appl. Surf. Sci.*, 2000, **162–163**, 565–570.

26 G. A. Somorjai, *Introduction of Surface Chemistry and Catalysis*, John Wiley & Sons, New York, 1994, pp. 445–447.

27 X. X. Fan, X. Y. Chen, S. P. Zhu, Z. S. Li, T. Yu, J. H. Ye and Z. G. Zou, *J. Mol. Catal. A: Chem.*, 2008, **284**, 155.

28 (*a*) J. Pera and D. F. Ollis, *J. Catal.*, 1992, **136**, 554–565; (*b*) C. Shifu, C. Xueli, T. Yaowu and Z. Mengyue, *J. Chem. Technol. Biotechnol.*, 1998, **73**, 264–268.

29 (*a*) D. Bahnemann, A. Henglein, J. Lilie and L. Spanhel, *J. Phys. Chem.*, 1984, **88**, 709; (*b*) D. Bahnemann, A. Henglein and L. Spanhel, *Faraday Discuss. Chem. Soc.*, 1984, **78**, 151; (*c*) A. Henglein, B. Lindig and J. Westerhausen, *J. Phys. Chem.*, 1981, **85**, 1627; (*d*) D. Bahnemann, J. Mönig and R. Chapman, *J. Phys. Chem.*, 1987, **91**, 3782–3788.

30 K. Uosaki, R. Yoneda and H. Kita, *J. Phys. Chem.*, 1985, **89**, 4042–4046.

31 V. Subramanian, E. E. Wolf and P. V. Kamat, *J. Phys. Chem. B*, 2003, **107**, 7479–7485.

32 (*a*) T. Hirakawa and P. V. Kamat, *Langmuir*, 2004, **20**, 5645; (*b*) T. Hirakawa and P. V. Kamat, *J. Am. Chem. Soc.*, 2005, **127**, 3928; (*c*) G. Oldfield, T. Ung and P. Mulvaney, *Adv. Mater.*, 2000, **12**, 1519.

33 J. Disdier, J. M. Herrmann and P. Pichat, *J. Chem. Soc., Faraday Trans.*, 1983, **79**, 651.

34 S. Yin, H. Hasegawa, D. Maeda, M. Ishitsuka and T. Sato, *J. Photochem. Photobiol., A*, 2004, **163**, 1.

35 (*a*) G. Balasubramanian, D. D. Dionysiou, M. T. Suidan, V. Subramanian, I. Baudin and J.-M. Laıne, *J. Mater. Sci.*, 2003, **38**, 823; (*b*) Y. Chen and D. D. Dionysiou, *Appl. Catal., B*, 2006, **69**, 24–33.

36 (*a*) V. Subramanian, R. K. Roeder and E. E. Wolf, *Ind. Eng. Chem. Res.*, 2006, **45**, 2187; (*b*) V. Subramanian, E. E. Wolf and P. V. Kamat, *Langmuir*, 2003, **19**, 469; (*c*) V. Subramanian, P. V. Kamat and E. E. Wolf, *Ind. Eng. Chem. Res.*, 2003, **42**, 2131–2138.

